SIAM REVIEW
Vol. 36, No. 3, pp. 453–469, September 1994

008

VISUALIZATION OF SPECIAL EIGENMODE SHAPES OF A VIBRATING ELLIPTICAL MEMBRANE*

GOONG CHEN†, PHILIP J. MORRIS‡, AND JIANXIN ZHOU†

Abstract. Analysis of eigenfunctions and eigenvalues of the Laplacian is important in the understanding of distributed parameter vibration systems and quantum mechanics. The elliptical domain is advantageous for such work because it allows the explicit representation of eigenfunctions as products of the Mathieu functions. In [*Ann. Phys.*, 9 (1960), pp. 24–75], Keller and Rubinow used wave propagation, geometrical optics, and WKB methods to show that two special types of eigenmodes, *whispering gallery* and *bouncing ball* modes, exist on a general convex domain, and they illustrated the case of an elliptical domain. In this paper, we develop a numerical package of the Mathieu and modified Mathieu functions to actually construct profiles of a sequence of eigenfunctions in order to visualize such special eigenmodes and others. In the process, we have also been able to observe a new type of transition state named "focusing modes" herein, which seem to have a complementary behavior to the bouncing ball modes. Numerical eigenvalues are tabulated for comparison and some discussions on the "focusing modes" are presented.

Key words. visualization, whispering gallery, bouncing ball and focusing modes, WKB, wave propagation, Mathieu functions

AMS subject classifications. 65N25, 73D30, 81C15, 34B30

1. Introduction.

The analysis of eigenfunctions and eigenvalues of the Laplacian is important in applications [5], [6]. Such a problem often arises from the separation of space and time variables either of the wave equation modelling a vibrating membrane and acoustic oscillations, or of the Schrödinger equation in quantum mechanics. We write the problem as

$$\text{(P)} \qquad \begin{cases} \text{Find } \phi_n\colon \Omega \to \mathbb{C} \text{ and } \lambda_n \in \mathbb{C} \text{ for } n = 1, 2, \ldots \text{ such that} \\ \Delta\phi_n(x) + \lambda_n^2 \phi_n(x) = 0 \quad \forall x \in \Omega, \\ \phi_n \text{ satisfies certian boundary conditions on } \partial\Omega. \end{cases}$$

In the above, Ω denotes a bounded open domain in $\mathbb{R}^N$ with sufficiently smooth boundary $\partial\Omega$, and $\mathbb{C}$ is the complex number field. Numerous articles on this problem have been published by researchers. One of the most outstanding papers among them was written by Keller and Rubinow (K–R) [8] in 1960. In that paper, K–R used wave propagation and the WKB expansion to estimate the eigenvalues and eigenfunctions of (P) and obtained highly accurate asymptotic solutions. (See also some more recent treatments in Babič and Buldyrev [2], and Ramm [12].) Qualitatively, K-R [8] also confirmed the existence of eigenmodes of certain special types, called the *whispering gallery* and *bouncing ball* modes. The whispering gallery mode in acoustics was first pointed out by Lord Rayleigh in 1910, who showed that at certain high frequencies sound waves exhibit a particle behavior like a ball sliding along the boundary of a circular domain. The (eigen)mode profile is essentially different from zero only in a thin strip adjacent to the boundary $\partial\Omega$, as shown in Fig. 1. Consequently, a person who speaks near the wall of a convex room can be heard across the room near the wall, but not in the interior of the room. Elsewhere in quantum mechanics, the normalized eigenfunction $\phi_n(x)$ in (P) signifies, for example, that the probability of finding an electron, with an energy level proportional to λ_n^2, in a subdomain $D \subset \Omega$ is $\int_D |\phi_n(x)|^2\, dx$. It is well known that at high energy levels, the

*Received by the editors June 24, 1992; accpeted for publication (in revised form) March 21, 1994

†Department of Mathematics, Texas A&M University, College Station, Texas 77843. This research was supported in part by Air Force Office of Scientific Research grant 91-0097.,

‡Department of Aerospace Engineering, Pennsylvania State University, University Park, Pennsylvania 16802. This research was supported in part by National Aeronautics and Space Administration grant NAG-1-657. The technical monitor is Dr. J. M. Seiner.

distribution of electrons (or "electron clouds") will be uneven in Ω, where one can "capture an electron" with the largest probability only on a proper subdomain of Ω. One type of such a subdomain is exhibited in Fig. 1, where a whispering gallery mode is manifest. Another type of subdomain, shown in Fig. 2, is formed by a thin strip around the line segment which is the shortest diameter of the domain. This is a *bouncing ball* mode displaying the behavior of a particle bouncing back and forth on the wall. The eigenfunction decays exponentially fast across the bounding curves of these strips in Figs. 1 and 2 and is negligibly small on the nonshaded regions (and thus called the *classically forbidden regions*). The bounding curves of these thin strips are formed by *caustics*. Both types of modes reflect a strong matter-wave dualism of electrons or other subatomic particles in quantum mechanics.

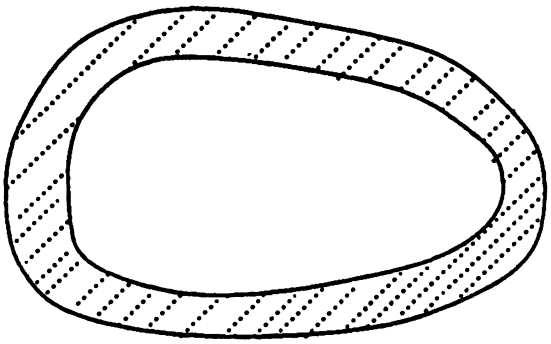

FIG. 1. *A whispering gallery mode. Such a mode is concentrated primarily in a thin strip adjacent to* $\partial\Omega$ *of a convex domain* Ω.

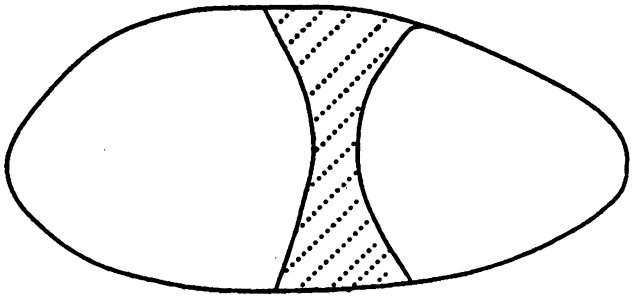

FIG. 2. *A bouncing ball mode. Such a mode is concentrated primarily in a thin strip adjacent to a minimum diameter of* Ω.

K-R [8] dealt with a general convex domain, but for special geometries such as circular, elliptical, rectangular and equilateral triangular domains in $\mathbb{R}^2$, K–R [8] showed explicitly how to estimate the eigenfunctions and eigenvalues asymptotically. As whispering gallery and bouncing ball modes form only a subgroup of the total set of eigenmodes, [8] also showed the conditions *when* they will occur on circular and elliptical domains. Nevertheless, the *actual shapes* of these modes have never been carefully *illustrated* until recently. In [4], the authors used the information from [8] to plot the profiles of some *whispering gallery modes* on a disk (cf. Figs. 5 and 6 therein) and further used the asymptotic properties of such modes to elucidate some mathematical theorems of a functional analysis nature. However, profiles of bouncing ball modes do not seem to have been plotted before (until now), to the best of our knowledge.

The lack of such graphical constructions is understandable. Bouncing ball modes do not exist on circular domains but rather on elliptical domains. They do not exhibit a sharp

bouncing ball property until the frequencies (or energy levels) become high. If one were to actually compute the eigenmodes and eigenvalues by the finite-element method, for example, one would encounter the difficulties of

(i) laborious work of computer coding;

(ii) loss of accuracy due to domain and boundary discretization; and

(iii) large computer memory and CPU time required in order to reach some asymptotic regime and high resolution for the occurrence of bouncing ball modes, since the finite-element method can only compute eigenvalues in ascending magnitudes sequentially.

To say the least, this is a rather burdensome assignment.

As *visualization* constitutes an important component in modern computer assisted research, in this paper we undertake the task of plotting the graphics of some eigenmodes on an elliptical domain with the particular objective of drawing the profiles of whispering gallery and bouncing ball modes thereupon. We take the direct classical approach of separation of variables using Mathieu functions, and develop the requisite numerical software for computation. In our opinion, this approach eases a great deal of computer program coding yet surely generates the highest possible numerical accuracy. In the process we have also been able to observe the profiles of a new family of modes, tentatively named *focusing modes* herein, which are related to the focusing phenomenon by the two foci of the ellipse, and occur when the eigen-states are in transition from a whispering gallery mode to a bouncing ball mode.

We hope that the graphics obtained and the computational methods developed herein will be useful to others in the research of vibration and wave propagation.

2. Eigenmodes on an elliptical domain. An elliptical domain, except for its symmetry, is just a convex domain. The eigenmodes on an elliptical domain are worth studying because they tend to provide qualitative information for a general convex domain. In particular, such a study is feasible, for we have the (luxury of) explicit representations as products of Mathieu functions. To limit the length of our exposition, except otherwise mentioned, throughout we assume that the boundary condition to be imposed in (P) is Dirichlet:

$$\phi_n(x)|_{\partial\Omega} = 0. \tag{2.1}$$

On the (x_1, x_2)-plane, we establish an elliptic coordinate system

$$\begin{cases} x_1 = \dfrac{c}{2}\cosh\mu\cos\theta, \\ x_2 = \dfrac{c}{2}\sinh\mu\sin\theta, \end{cases} \tag{2.2}$$

where c is a positive constant, $0 < \mu < \infty$ and $0 \le \theta \le 2\pi$. The curves $\mu =$ constant and $\theta =$ constant are, respectively, confocal ellipses and hyperbolas. We let Ω be an open domain bounded by the ellipse $\mu = R_0$. Then this ellipse satisfies

$$\frac{x_1^2}{A^2} + \frac{x_2^2}{B^2} = 1,$$

where A and B are, respectively, the length of the major and minor axis of the ellipse, with

$$\begin{cases} A = \dfrac{c}{2}\cosh R_0, \\ B = \dfrac{c}{2}\sinh R_0. \end{cases} \tag{2.3}$$

The foci of the ellipse are located at $x_1 = \pm c/2$.

Using elliptic coordinates, we can separate the variables for the Helmholtz equation

$$\frac{\partial^2}{\partial x_1^2} w(x_1, x_2) + \frac{\partial^2}{\partial x_2^2} w(x_1, x_2) + k^2 w(x_1, x_2) = 0. \tag{2.4}$$

First, from (2.2),

$$\frac{8}{c^2(\cosh 2\mu - \cos 2\theta)} \left(\frac{\partial^2 w}{\partial \mu^2} + \frac{\partial^2 w}{\partial \theta^2} \right) + k^2 w = 0. \tag{2.5}$$

Assume a solution of the form

$$w = f(\mu) g(\theta).$$

Substituting the above into (2.5) and dividing by fg, we obtain

$$8 \left(\frac{f''}{f} + \frac{g''}{g} \right) + k^2 c^2 (\cosh 2\mu - \cos 2\theta) = 0.$$

Letting

$$\alpha = 8 \left(\frac{f''}{f} \right) + k^2 c^2 \cosh 2\mu, \qquad \alpha = -8 \left(\frac{g''}{g} \right) + k^2 c^2 \cos 2\theta,$$

we obtain two differential equations:

$$f''(\mu) - (a - 2q \cosh 2\mu) f(\mu) = 0, \tag{2.6}$$

$$g''(\theta) + (a - 2q \cos 2\theta) g(\theta) = 0, \tag{2.7}$$

where

$$a = \frac{\alpha}{8}, \qquad q = \frac{1}{16} k^2 c^2. \tag{2.8}$$

Equations (2.6) and (2.7) are said to be the *canonical form* of, respectively, the *modified Mathieu equation* and the *Mathieu equation.*

In [8], K–R use the notation $\mathcal{S} = \mathcal{S}(h, \cos\theta)$ for the Mathieu function, satisfying

$$\mathcal{S}'' + (b - h^2 \cos^2 \theta) \mathcal{S} = 0. \tag{2.9}$$

In our opinion, the choice of this notation $\mathcal{S}(h, \cos\theta)$ is best corrected to $\mathcal{S}(h, \theta)$ because $\mathcal{S}$ *depends on* θ *rather than* $\cos\theta$. (As a matter of fact, K–R made an error in their calculations because of their choice of notation, as we will point out later.) From now on we will write $\mathcal{S}(h, \theta)$ instead.

Since $\cos^2\theta = (\cos 2\theta + 1)/2$, we have

$$\mathcal{S}'' + \left[\left(b - \frac{h^2}{2} \right) - \frac{h^2}{2} \cos 2\theta \right] \mathcal{S} = 0. \tag{2.10}$$

Comparing (2.10) with (2.7), we get

$$\mathcal{S}'' + \left[\frac{1}{8} (\alpha + k^2 c^2) - \frac{1}{4} k^2 c^2 \cos^2 \theta \right] \mathcal{S} = 0, \tag{2.11}$$

$$a = b - \frac{h^2}{2}, \quad q = \frac{h^2}{4}, \quad h = \frac{kc}{2}. \tag{2.12}$$

For the modified Mathieu function, K–R use the notation $J(h, \cosh\mu)$, satisfying

$$J'' - (b - h^2\cosh^2\mu)J = 0. \tag{2.13}$$

For the same reason, we change their notation $J(h, \cos\mu)$ to $J(h, \mu)$.

Additional conditions are now imposed on $\mathcal{S}$ and J. First of all, we require that $\mathcal{S}$ in (2.9) be periodic in θ with period 2π. Thus for given h, only a countable set of values $b_m(h)$, $m = 1, 2, 3, \ldots$, are admissible in (2.9). Second, we add initial conditions

$$\mathcal{S}e(h, 0) = 1, \quad \mathcal{S}e'(h, 0) = 0, \tag{2.14}$$

$$\mathcal{S}o(h, 0) = 0, \quad \mathcal{S}o'(h, 0) = 0. \tag{2.15}$$

The subscripts "e" and "o" are intended to signify the "evenness" and "oddness" properties. Indeed, $\mathcal{S}e$ and $\mathcal{S}o$, subject to (2.9), (2.14), and (2.15), become even and odd functions of θ, respectively.

On the other hand, let us return to (2.7). For problems of physical interest, we mainly desire solutions of (2.7) that are periodic of period 2π and π. In [1,11], such even and odd periodic functions are denoted by $ce_{2n}(\theta, q)$, $ce_{2n+1}(\theta, q)$, $se_{2n}(\theta, q)$, and $se_{2n+1}(\theta, q)$, satisfying (2.7) and

$$\begin{aligned}
&ce_{2n}(\theta + \pi, q) = ce_{2n}(\theta, q), \qquad se_{2n}(\theta + \pi, q) = se_{2n}(\theta, q),\\
&ce_{2n+1}(\theta + 2\pi, q) = ce_{2n+1}(\theta, q), \; se_{2n+1}(\theta + 2\pi, q) = se_{2n+1}(\theta, q),\\
&ce_m(-\theta, q) = ce_m(\theta, q), \qquad m = 2n \text{ or } 2n + 1,\\
&se_m(-\theta, q) = -se_m(\theta, q), \qquad m = 2n \text{ or } 2n + 1.
\end{aligned}$$

The corresponding modified Mathieu functions as solutions of (2.6) are defined by

$$\left.\begin{aligned} Ce_m(\mu, q) &= ce_m(i\mu, q),\\ Se_m(\mu, q) &= se_m(i\mu, q), \end{aligned}\right\} \qquad m = 2n \text{ or } 2n + 1, \tag{2.16}$$

according to the notation in [1], and [11]. Comparing the notation between (the corrected) K–R and [1], [11], we have

$$\left.\begin{aligned} \mathcal{S}e_m &= \beta_m \cdot ce_m,\\ \mathcal{S}o_m &= \beta'_m \cdot se_m, \end{aligned}\right\} \quad m = 2n \text{ or } 2n + 1, \qquad n = 0, 1, 2, \ldots, \tag{2.17}$$

and

$$\begin{aligned} Je_m &= \beta''_m Ce_m,\\ Jo_m &= \beta'''_m Se_m, \end{aligned} \qquad m = 2n \text{ or } 2n + 1, \quad n = 0, 1, 2, \ldots, \tag{2.18}$$

where β_m, β'_m, β''_m, and β'''_m are constants of proportionality. (Actually, $\beta'_m = 1$ for all m.)

For each integer $m \geq 0$, we have eigenfunctions

$$w(x_1, x_2) = ce_m(\theta, q)Ce_m(\mu, q) \quad \text{or} \quad se_m(\theta, q)Se_m(\mu, q). \tag{2.19}$$

The first type on the right-hand side above is an even function of x:

$$w(-x_1, -x_2) = w(x_1, x_2),$$

while the second type is an odd function of x.

We determine the eigenvalues λ_n^2 in (P) as follows. Note that $\lambda_n^2 = k^2$ by comparing with (2.4). Assume that the boundary of the elliptical domain is defined by (2.3), whereupon the zero Dirichlet condition (2.1) holds. From (2.17)–(2.19), we have

$$\begin{aligned} w &= \gamma_m Se_m(h,\theta) Je_m(h,\mu) \\ &= \gamma_m Se_m\left(\frac{kc}{2},\theta\right) Je_m\left(\frac{kc}{2},\mu\right), \quad \text{(by (2.12))} \\ &= \gamma'_m ce_m\left(\theta,\frac{kc}{2}\right) Ce_m\left(\mu,\frac{kc}{2}\right) \end{aligned} \tag{2.20}$$

and

$$\begin{aligned} w &= \gamma''_m So_m\left(\frac{kc}{2},\theta\right) Jo_m\left(\frac{kc}{2},\mu\right) \\ &= \gamma'''_m se_m\left(\theta,\frac{kc}{2}\right) Se_m\left(\mu,\frac{kc}{2}\right), \end{aligned} \tag{2.21}$$

where γ_m, γ'_m, γ''_m, and γ'''_m, are constants. The boundary condition (2.1) imposes

$$Je_m\left(\frac{kc}{2}, R_0\right) = 0 = Ce_m\left(R_0,\frac{kc}{2}\right) \tag{2.22}$$

and

$$Jo_m\left(\frac{kc}{2}, R_0\right) = 0 = Se_m\left(R_0,\frac{kc}{2}\right) \tag{2.23}$$

for $m = 2n$ or $2n+1$, $n = 0, 1, 2, \ldots$. (If, instead of (2.1), the zero Neumann condition

$$\frac{\partial}{\partial n}\phi_n(x)|_{\partial\Omega} = 0$$

takes place, we would require

$$Je'_m\left(\frac{kc}{2}, R_0\right) = 0.$$

or

$$Jo'_m\left(\frac{kc}{2}, R_0\right) = 0,$$

in lieu of (2.22) and (2.23).) Since R_0 is given, from (2.22) and (2.23), we solve for q. Once q is determined and ranked in ascending order, we have from (2.8)

$$k^2 = \frac{16q}{c^2}.$$

Thus the eigenvalues $\lambda_n^2 = k^2$ are determined. In our numerical calculations, the modified Mathieu functions Ce_m and Se_m in (2.22) and (2.23) are computed from a recurrence relation given in [1, (20.2.5)–(20.2.10), p. 723], truncated to a matrix eigenvalue problem to yield a finite Bessel function product series. A concise description of the algorithm is provided in §V. The search of the roots q of (2.22) and (2.23) is done by combining a modified Newton's algorithm for roots with a quadratic interpolation method.

3. Numerical results and graphics. In our calculations, we choose $R_0 = 2$, $c = 2$. This choice of $R_0 = 2$ is made in order to compare the eigenvalues with those obtained by K–R. (K–R have chosen R_0 to satisfy $\cosh R_0 = 2$. Actually, what they did was to make $\mu_0 = R_0 = 2$, due to the way their notation was chosen as we mentioned after (2.9) and (2.13), leading to the confusion.) For the truncation of the series, see (5.13) later, terms within (and including) indices $r = 0$ and $r = 29$ are retained. The results are given as follows.

3.1. Approximate eigenvalues of the Laplacian. Computations of eigenvalues of the Laplacian on elliptical domains have been done by quite a few people, e.g., Hettich et. al. [7] and the references therein. Our source of comparison is Table II in [8, p. 42]. Note that for the Dirichlet condition $w = 0$ on $\partial\Omega$, the second (i.e., lower) table therein should be consulted rather than the first one [9]. As in [8], we tabulated the values of $kc/2$ instead of the eigenvalues k^2 themselves. See our Table 1. The magnitude and sequential orders of our values are very consistent with those given by K–R. Nevertheless, they don't agree in the detailed accuracy. Let us just examine the first row of Table 1. According to our calculations, the lowest eigenvalue of the Laplacian has

$$\frac{kc}{2} = 0.65123129,$$

because the corresponding eigenfunction is the only one with constant sign [3, Cor. 2, p. 20]. K–R have missed such a value. The second value $kc/2 = 1.49784709$ has similarly been missed by K–R. For the 7th value, we have 5.81293420 and 5.74569056, differing from K–R's value 5.919 by a relative accuracy of 3%. Some other entries in the table differ with an even larger relative percentage.

TABLE 1

Values of $\frac{kc}{2}$ satisfying $Ce_m(R_0, \frac{kc}{2}) = 0$ or $Se_m(R_0, \frac{kc}{2}) = 0$, with $R_0 = 2$, and comparison with the tabulated values by Keller and Rubinow [4, Table II]. *K–R gave only the part of their table above and on the main diagonal. The lower triangular part of their table may be computed by a different formula which they chose not to use.*

Ce_0	0.65123129	1.49784709	2.35503473	3.21749843	4.08203626	4.94732655	5.81293420
Se_0			2.28073760	3.15122897	4.01676288	4.88119330	5.74569056
$K-R$	M	M	2.356	3.220	4.121	5.019	5.919
Ce_1	1.02808007	1.88388127	2.73593640	3.59120982	4.45108722	5.31394317	6.17818679
Se_1		1.918336066	2.78409872	3.64927690	4.51451132	5.38008810	6.24580307
$K-R$	M	M	2.709	3.927	4.792	5.677	6.569
Ce_2	1.38747716	2.26882701	3.12071201	3.97901797	4.83233029	5.68947133	6.55017404
Se_2		2.25732054	3.11618100	3.96794909	4.81647132	5.66328950	6.50920610
$K-R$	M	M	3.380	M	M	5.498	6.358
Ce_3	1.72602682	2.63820326	3.51256008	4.37137203	5.22392323	6.07591028	6.93070787
Se_3		2.64047268	3.52057041	4.38936670	5.25397297	6.11736414	6.98077503
$K-R$	M	M	M	4.029	M	5.856	7.069
Ce_4	2.05326667	2.99268174	3.88482175	4.75670222	5.61649357	6.46963028	7.32089967
Se_4	2.27770674	3.14260402	3.99863927	4.84906259	5.69457215	6.53473244	7.36814414
$K-R$	M	M	M	4.663	M	6.549	M
Ce_5	2.37354250	3.33789874	4.24766336	5.13015750	6.00083927	6.86162867	7.71565474
Se_5	2.37354419	3.38792570	4.24597551	5.13123884	6.00462089	6.87133728	7.73452313
$K-R$	M	M	M	5.323	M	7.224	M
Ce_6	2.68877593	3.67658809	4.59920950	5.49462839	6.37490204	7.24488261	8.10659707
Se_6	3.14538710	4.00495543	4.86085219	5.71422751	6.56520281	7.41315641	8.25650774
$K-R$	M	M	M	5.902	M	M	7.886

M: values not provided

3.2. Graphics of the whispering gallery modes. The whispering gallery modes are of the form (2.20) or (2.21), where for given m, $kc/2$ is the smallest root of the transcendental

equation (2.22) and (2.23), respectively. Such values of $kc/2$ are listed on the leftmost column of Table 1. (In particular, K-R's table have not provided any whispering gallery modes.) We have plotted the graphs of a whispering gallery mode

$$w = \gamma \cdot ce_{11}(\theta, 4.21899612)Ce_{11}(\mu, 4.21899612)$$

in Fig. 3. Readers can clearly observe that prominent vibrations happen near the boundary $\partial\Omega$, as indicated in Fig. 1. In Fig. 3 the number of peaks along the peripheral is 11. They signify the angular dependence 11 in the order of Mathieu functions ce_{11}, respectively.

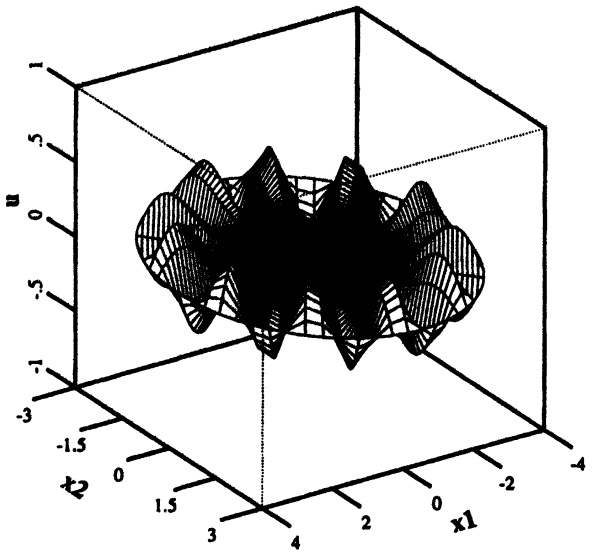

FIG. 3. *Whispering gallery mode* $ce_{11}(\theta, 4.21899612)Ce_{11}(\mu, 4.21899612)$.

3.3. Graphics of a sequence of eigenmodes corresponding to Mathieu functions of a fixed order. We first compute the roots q_n of the canonical Mathieu function of order 11

$$Ce_{11}\left(R_0, \frac{k_n c}{2}\right) = 0, \quad n = 1, 2, \ldots, 28. \qquad \text{(cf. (2.22))}.$$

The first twenty-eight such values $k_n c/2$ are listed in Table 2. Some of the corresponding eigenfunctions are plotted sequentially in Figs. 3-8. We mention some of their special features below.

(i) Figure 3, with $n = 1$, is a whispering gallery mode already mentioned in the previous section (3.2).

(ii) Figures 4 and 5: we let n increase. More radial oscillations are observed. (Figs. 4 and 5 correspond, respectively, to $n = 5$ and 9.) They eventually fill up the entire ellipse except for a thin strip surrounding the interfocal line.

(iii) Figures 6 and 7: as n further increases, we see the presence of internal wave propagating longitudinally. Some of them are what we call "focusing modes." See §IV. Figures 6 and 7 correspond to $n = 15$ and 19, respectively.

(iv) As n increases past 19, we see the onset of the "bouncing ball" phenomenon. The eigenmodes become flatter and flatter on two strips along the major axis outside the interfocal line. In Fig. 8, corresponding to $n = 28$, the eigenmode manifests a pattern just as indicated in Fig. 2.

TABLE 2
The first 28 *roots* $\frac{kc}{2}$ *of* $Ce_{11}\left(R_0, \frac{kc}{2}\right) = 0$, *with* $R_0 = 2$.

1	4.21899612
2	5.30803620
3	6.29769953
4	7.24310924
5	8.16335720
6	9.06741194
7	9.96018976
8	10.84465048
9	11.72268331
10	12.59552397
11	13.46394683
12	15.18861872
13	16.04463995
14	16.89680217
15	17.74669045
16	18.59652509
17	19.44813867
18	20.30256734
19	21.15887304
20	22.01721538
21	22.87529043
22	23.73708949
23	24.58998617
24	25.46713863
25	26.30879068
26	27.19408193
27	28.03255254
28	28.90509607

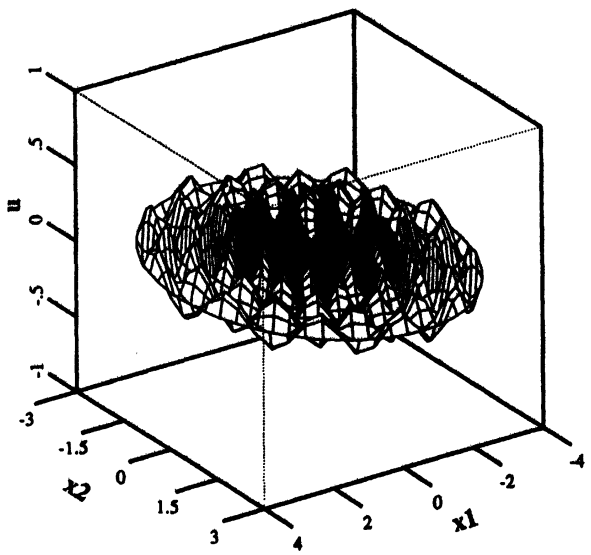

FIG. 4. *Eigenmode* $ce_{11}(\theta, k_5c/2)Ce_{11}(\mu, k_5c/2)$, $k_5c/2 = 8.16335720$.

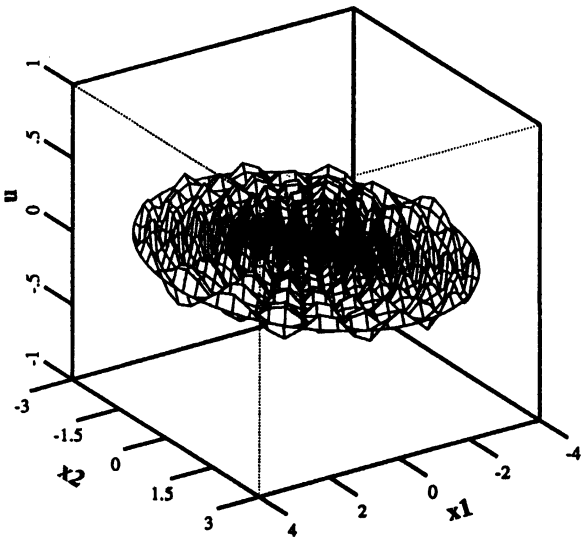

FIG. 5. *Eigenmode* $ce_{11}(\theta, k_9c/2)Ce_{11}(\mu, k_9c/2)$, $k_9c/2 = 11.72268331$.

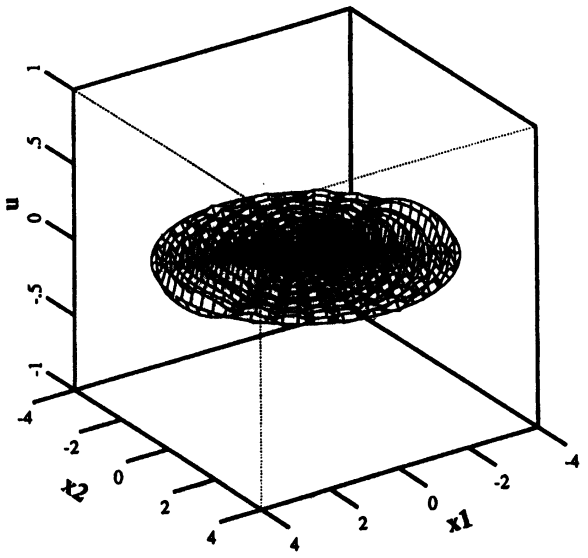

FIG. 6. *Eigenmode* $ce_{11}(\theta, k_{15}c/2)Ce_{11}(\mu, k_{15}c/2)$, $k_{15}c/2 = 17.74669045$.

In order to make comparison, we have plotted a bouncing ball mode of Mathieu functions of order 1:

$$ce_1\left(R_0, \frac{k_nc}{2}\right)Ce_1\left(R_0, \frac{k_nc}{2}\right) = 0, \quad n = 16, \quad \frac{k_nc}{2} = 13.9685.$$

See Fig. 9. For this mode, the strip whereupon the eigenmode is concentrated is narrower, corresponding to a sharper bouncing ball behavior. The reason is that the ratio

$$\frac{4m+2}{n}$$

is smaller (with $m = 1, n = 16$) than the case in Fig. 8 (with $m = 11, n = 28$), consistent with the estimate in [8, (95), p.50]. The change of the pattern is indicated in Fig. 10.

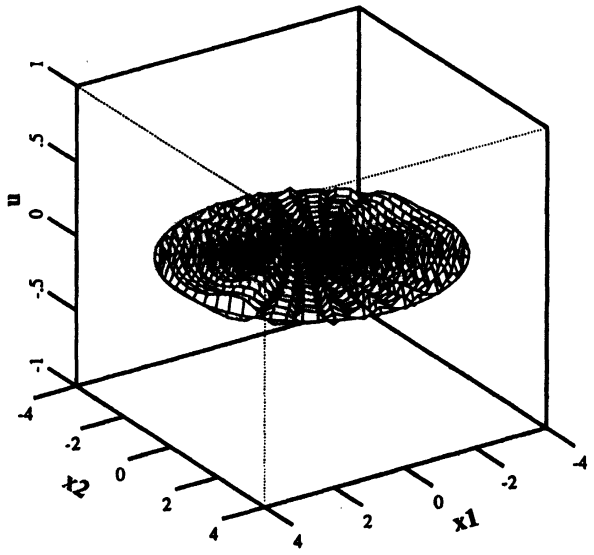

FIG. 7. *Eigenmode* $ce_{11}(\theta, k_{19}c/2)Ce_{11}(\mu, k_{19}c/2)$, $k_{19}c/2 = 21.15887304$.

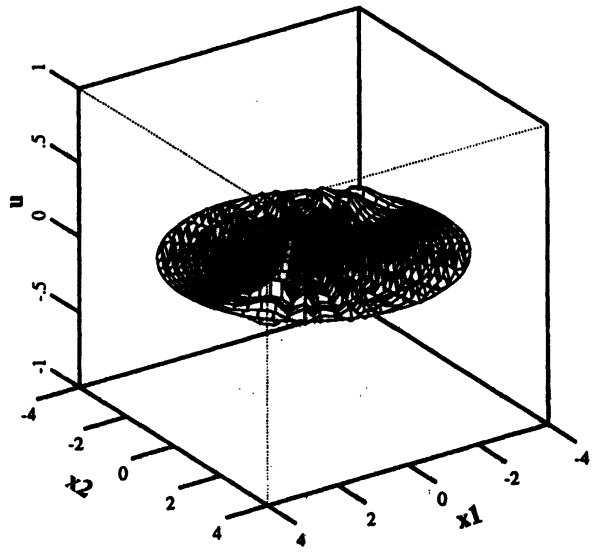

FIG. 8. *Eigenmode* $ce_{11}(\theta, k_{28}c/2)Ce_{11}(\mu, k_{28}c/2)$, $k_{28}c/2 = 28.90509607$.

Empirically, for eigenmodes

$$\gamma_m \cdot ce_m\left(\theta, \frac{k_n c}{2}\right) Ce_m\left(\mu, \frac{k_n c}{2}\right) \tag{3.1}$$

or

$$\gamma_m' \cdot se_m\left(\theta, \frac{k_n c}{2}\right) Se_m\left(\mu, \frac{k_n c}{2}\right) \tag{3.2}$$

given in (2.20) and (2.21), fixing m and *letting n become large*, we have found that *they have all become bouncing ball modes*, consistent with [8, (95), p.50].

4. Comments on focusing modes. In addition to graphically confirming the whispering gallery and bouncing ball modes on an elliptical domain, we would like to point out that we

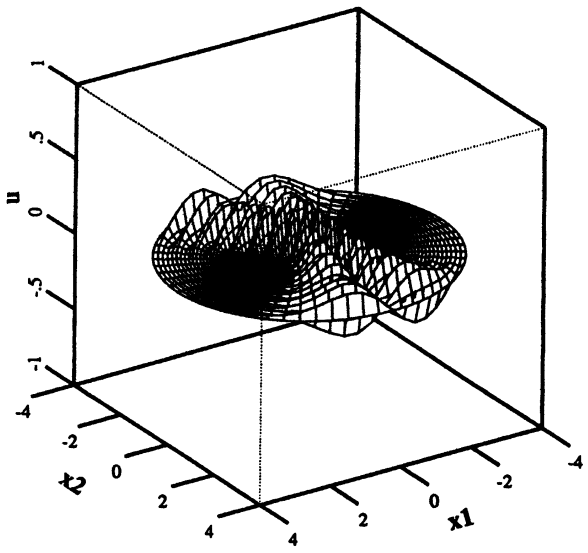

FIG. 9. *Eigenmode* $ce_{11}(\theta, k_n c/2)Ce_{11}(\mu, k_n c/2), k_n c/2 = 17.74669045.$

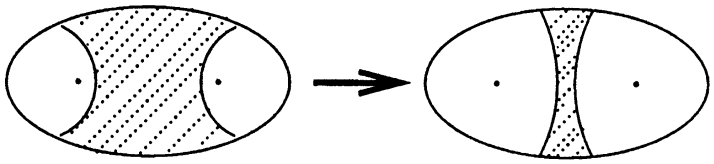

FIG. 10. *The width of a bouncing ball mode narrows as* $(4m + 2)/n$ *becomes small.*

are also able to observe the focusing phenomenon in the sequence of computer graphics given in §III.

The focusing phenomenon itself is quite well understood in classical optics. We first look at the case of a circular disk; see Fig. 11. If a source is concentrated near the center of the disk, then a family of divergent rays passing through the center is reflected backward by the circle and converges at the center, forming a small area of high intensity. As eigenfunctions, such focusing modes on a disk are represented by

$$\phi(x) = J_0(\lambda_{0,n} r), \qquad r = |x| \leq R,$$

where J_0 is the Bessel function of order 0, $\lambda_{0,n}$ is the nth positive root of $J_0(\lambda_{0,n} R) = 0$, R is the radius of the disk and the zero Dirichlet condition is assumed in effect in (P). We have plotted a focusing mode $w(x) = J_0(\lambda_{0,20} r)$ in Fig. 12. Note that no caustics exist for a focusing mode. The focusing mode seems to be *complementary* to all other eigenmodes of the form

$$\phi(x) = J_m(\lambda_{mn} r) e^{\pm im\theta}, \quad m, n \geq 1, \quad r = |x| \leq R, \quad \theta = \arg x,$$

which have angular dependence and a profile with a *flat* circular region around the center of the disk; see [4, Figs. 5–7]. K–R's eigenvalue analysis is based upon the presence of caustics. The presence of *strong singularities* such as *foci* has not been taken into account. Yet it is amazing to note that the derived equations [8, eqs. (23) and (26)] remain valid even for the focusing modes whereupon there are no caustics. A simple explanation offered here is that equations (23) and (26) in [8] remain valid because of *analytic continuation.*

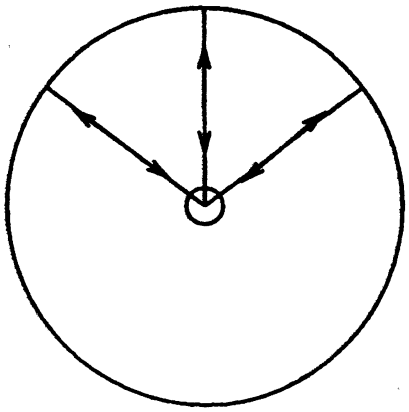

FIG. 11. *The focusing phenomenon on a circular disk.*

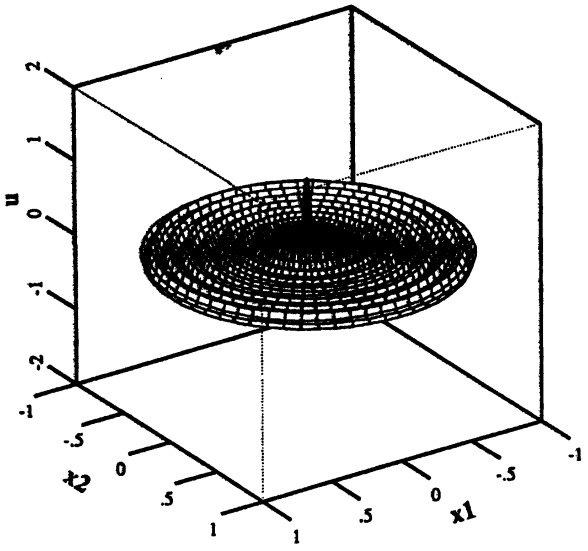

FIG. 12. *A focusing mode* $w(x) = J_0(\lambda_{0,20}r)$, $r = |x|$, *with* $\lambda_{0,20} = 62.04846$, *on a unit disk.*

On an elliptical domain, the way in which rays converge at the foci is shown in Fig. 13. Figure 7 is actually a "focusing mode." This is better explained if we make an "optical processing" of "filtering": All the computer graphics in Figs. 3–12 are plotted using the resolution of 60×60 dots for $0 \leq \theta \leq 2\pi$ and $0 \leq \mu \leq 2$. Now for Fig. 7, if we plot that eigenmode using a coarser resolution of 40×40 dots, then minor oscillations are obscured (i.e., filtered), and we obtain a new Fig. 14 for the same eigenmode, wherein one may clearly observe peaks near the foci area and where waves seem to converge. Therefore such a mode can rightfully be called a "focusing mode." Note that areas of concentration of this mode appear to be *complementary* to that of a bouncing ball mode.

5. Calculation of the modified Mathieu functions and Mathieu functions. The modified Mathieu functions are calculated first according to the following sequence:

(1) The characteristic numbers and the associated coefficients are obtained from the recurrence relationships for the coefficients;

(2) The coefficients are normalized;

(3) A solution is sought in the form of a Bessel function product series;

(4) The amplitude of the summed series is modified to conform with the preferred series definitions for the modified Mathieu functions.

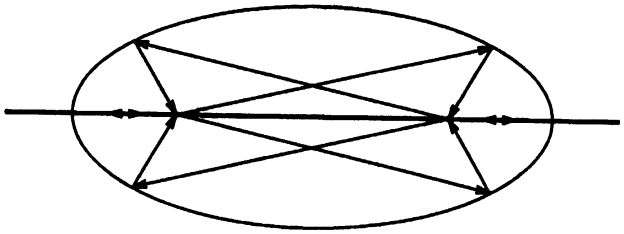

FIG. 13. *Rays converge at the foci of an ellipse.*

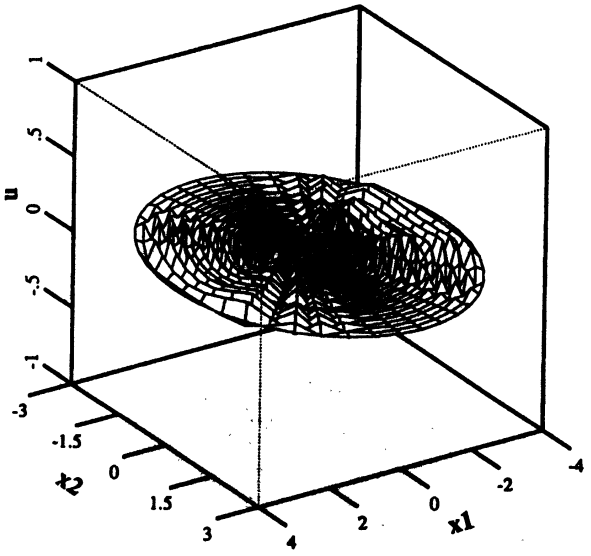

FIG. 14. *A "focusing mode." This mode is the same eigenfunction* $ce_{11}(\theta, k_{19}c/2)Ce_{11}(\mu, k_{19}c/2)$ *as shown in Fig. 7, except that it is plotted on a coarser* 40×40 *resolution. This corresponds to a filtering optical treatment. Sharp peaks are found near the foci, suggesting the focusing of rays.*

A detailed derivation of the formulas used in these calculations is contained in McLachlan [11] and useful formulas are also given by Abramowitz and Stegun [1]. There are small differences between the formulas used in the calculations of the four classes of modified Mathieu functions. For simplicity, only the calculation of the $Ce_{2n}(z, q)$ function will be described in any detail. The similar formulas for the $Ce_{2n+1}(z, q)$, $Se_{2n+1}(z, q)$, and $Se_{2n+2}(z, q)$ functions can be found in [1] and [11].

5.1. Calculation of the characteristic numbers and coefficients. The Mathieu and modified Mathieu equations may be written as

$$\frac{d^2y}{dz^2} + (a - 2q\cos 2z)y = 0 \tag{5.1}$$

and

$$\frac{d^2y}{dz^2} - (a - 2q\cosh 2z)y = 0, \tag{5.2}$$

respectively. The preferred form of series for the Mathieu functions are [11, §2.17],

$$ce_{2n}(z, q) = \sum_{r=0}^{\infty} A_{2r}^{(2n)} \cos 2rz, \tag{5.3}$$

$$ce_{2n+1}(z,q) = \sum_{r=0}^{\infty} A_{2r+1}^{(2n+1)} \cos(2r+1)z, \tag{5.4}$$

$$se_{2n+1}(z,q) = \sum_{r=0}^{\infty} B_{2r+1}^{(2n+1)} \sin(2r+1)z, \tag{5.5}$$

and

$$se_{2n+2}(z,q) = \sum_{r=0}^{\infty} B_{2r+2}^{(2n+2)} \sin(2r+2)z, \tag{5.6}$$

ce_{2n} and ce_{2n+1} are even functions of z with period π are 2π, respectively, se_{2n+1} and se_{2n+2} are odd functions of z with period π and 2π, respectively. The corresponding series for the modified Mathieu functions are in terms of hyperbolic functions since

$$Ce_{2n}(z,q) = ce_{2n}(iz,q). \tag{5.7}$$

The series coefficients and the characteristic numbers are identical. The recurrence relationships for the coefficients may be obtained by substitution of the preferred series forms in (5.1). If the recurrence relationships are truncated after N terms they form a system of homogeneous, simultaneous equations for the coefficients. The equations may be written as an algebraic eigenvalue problem in which the eigenvalues are the characteristic numbers. In the present calculations the eigenvalues and the eigenvectors are obtained using the IMSL routine EIGCC. For $N = 11$ (i.e., $0 \le r \le 10$ in (5.3) and (5.4)) the lowest characteristic numbers agreed with those tabulated by Abramowitz and Stegun [1] to 8 decimal places. The eigenvectors $A_{2r}^{(2n)}$ were found to agree to the same order of accuracy. However, in order to satisfy the normalization convention for the Mathieu functions that [11, §2.21]

$$\frac{1}{\pi}\int_0^{2\pi} ce_m^2(z,q)dz = \frac{1}{\pi}\int_0^{2\pi} se_m^2(z,q)dz = 1, \tag{5.8}$$

the eigenvectors for the Ce_{2n} function must be normalized such that

$$2[A_0^{(2n)}]^2 + \sum_{r=0}^{\infty}[A_{2r}^{(2n)}]^2 = 1. \tag{5.9}$$

Similar normalization conditions are applied to the other classes of Mathieu function series coefficients.

If a series solution is sought to (5.2) of the form [11, §13.10]

$$y = \sum_{r=-\infty}^{r=\infty} (-1)^r d_{2r} J_r(v_1) J_{r+\nu}(v_2), \tag{5.10}$$

where

$$v_1 = ke^z \quad \text{and} \quad v_2 = ke^{-z} \quad \text{for } k^2 = q, \tag{5.11}$$

and J_r is the Bessel function of the first kind of order r, it is found that the recurrence relationships for d_{2r} are identical to those for $A_{2r}^{(2n+\nu)}$. Hence for the same a and q, if $d_{2r} = K_{2n+\nu}A_{2r}^{(2n+\nu)}$, $K_{2n+\nu}$ being a constant, it follows that

$$y = K_{2n+\nu} \sum_{r=-\infty}^{r=\infty} (-1)^r A_{2r}^{(2n+\nu)} J_r(v_1) J_{r+\nu}(v_2) \tag{5.12}$$

is a solution of (5.2). Series solutions that are odd or even in z may be obtained by setting $z = -z$ in (5.12) and adding or subtracting the resulting series from (5.12). The values of $K_{2n+\nu}$ are obtained by matching the Bessel function product series representation with the asymptotic forms for the modified Mathieu functions [11, §13.11, 13.12]. Thus, for example,

$$Ce_{2n}(z, q) = \frac{p_{2n}}{A_0^{(2n)}} \sum_{r=0}^{r=\infty} (-1)^r A_{2r}^{(2n)} J_r(v_1) J_r(v_2), \tag{5.13}$$

where [11, Appendix I, §3]

$$p_{2n} = ce_{2n}(0, q) ce_{2n}(\pi/2, q) A_0^{(2n)}. \tag{5.14}$$

Solutions of the third kind, equivalent to Hankel functions, may be obtained in a similar manner. For example,

$$Me_{2n}^{(1)} = \frac{p_{2n}}{A_0^{(2n)}} \sum_{r=0}^{r=\infty} (-1)^r A_{2r}^{(2n)} J_r(v_1) H_r^{(1)}(v_2), \tag{5.15}$$

where, $H_r^{(1)}$ is the Hankel function of the first kind and order r. Finally, it should be noted that the derivatives of the modified Mathieu functions may be obtained by differentiation of the Bessel function product series. In their present form, the modified Mathieu function subroutines also evaluate the derivative with respect to the function's argument.

In the present calculations of the modified Mathieu functions the Bessel function product series was summed until the magnitude of the ratio of the next term in the series to the partial sum was less than 10^{-8}. In general only five terms in the series were needed. The values of $ce_{2n}(0, q)$ and $ce_{2n}(\pi/2, q)$ required in (5.13) and (5.14) are determined from the series coefficients using (5.3). The Bessel function product series was evaluated for wide range of values of z and q. The results have been compared with the values tabulated by Kirkpatrick [10] and agreed to the accuracy of those computations. See Table 3. As further checks on the validity of the calculations, the following result was tested numerically:

$$Ce_0(z, -q) = Ce_0(z + i\pi/2, q), \tag{5.16}$$

and was found to be satisfied. Finally, the modified equation was integrated numerically using initial conditions generated by the modified Mathieu functions subroutines. The results at the end of the range of integration were compared with the series approximations. The results agreed, for both the function and its derivative to 8 significant figures. Thus considerable confidence may be placed in the accuracy of the modified Mathieu function subroutines. Using (5.7), we easily obtain the canonical Mathieu functions ce_n and se_n.

Final note added. After the acceptance of this paper, Prof. Joseph B. Keller of Stanford University sent us a collection of unpublished numerical data of eigenvalues of Δ on elliptical domains with different eccentricities and boundary conditions. The computational work was carried out by Prof. Eugene Issacson and his students at the Courant Institute of Mathematical Sciences of New York University during the sixties. Their results, computed from Mathieu functions, are also very accurate. Their data have shown some fractional difference from the corresponding eigenvalues computed from the asymptotic formulas Keller and Rubinow have derived. They have found no case in which those asymptotic formulas fail. We mention this fact to further complement the list of references provided below. We also wish to thank Prof. Keller for communicating this to us.

TABLE 3

Comparison of numerical values of the modified Mathieu function $Ce_5(1, q)$, *obtained by our algorithms in* §5 *(middle column) and by E. T. Kirkpatrick* [10, *Table* 6] *(third column).*

q		
1	54.60629927	54.6063
2	39.51952105	39.5195
3	28.02845421	29.0285
4	19.37904040	19.3790
5	12.95741669	12.9574
6	8.26755682	8.2676
7	4.91210250	4.9121
8	2.57540926	2.5754
9	1.00823869	1.0082
10	0.01416872	0.01418
12	-0.84047602	-0.84049
14	-0.86017691	-0.86016
16	-0.54740402	-0.54741
18	-0.17203806	-0.17196
20	0.12766301	-0.12777

Acknowledgment. We wish to thank Professors S. A. Fulling, F. J. Narcowich and G. C. Papanicolaou for extremely helpful discussions.

REFERENCES

[1] M. ABRAMOWITZ AND I. A. STEGUN, *Handbook of Mathematical Functions*, Dover, New York, 1965.
[2] V. M. BABIČ AND V. S. BULDYREV, *Short Wave Length Diffraction Theory*, Springer-Verlag, New York, 1991.
[3] I. CHAVEL, *Eigenvalues in Riemannian Geometry*, Academic Press, New York, 1984.
[4] G. CHEN, S. A. FULLING, F. J. NARCOWICH, AND S. SUN, *Exponential decay of energy of evolution equations with locally distributed damping*, SIAM J. Appl. Math., 51 (1991), pp. 266–301.
[5] G. CHEN AND J. ZHOU, *Vibration and Damping in Distributed Systems, Vol.* I: *Analysis, Estimation, Attenuation and Design*, CRC Press, Boca Raton, FL, 1993.
[6] ———, *Vibration and Damping in Distributed Systems, Vol.* II: *WKB and Wave Methods, Visualization and Experimentation*, CRC Press, Boca Raton, FL, 1993.
[7] R. HETTICH, E. HAAREN, M. RIES, AND G. STILL, *Accurate numerical approximations of eigenfrequencies and eigenfunctions of elliptic membranes*, ZAMM, 67 (1987), pp. 589–597.
[8] J. B. KELLER AND S. I. RUBINOW, *Asymptotic solution of eigenvalue problems*, Ann. Phys., 9 (1960), pp. 24–75.
[9] ———, Errata (to [4] above), Ann. Phys., 10 (1960), pp. 303–305.
[10] E. T. KIRKPATRICK, *Tables of values of the modified Mathieu function*, Math. Comp., 14 (1960), pp. 118–129.
[11] N. W. MCLACHLAN, *Theory and Application of Mathieu Functions*, Oxford University Press, 1947.
[12] A. G. RAMM, *Scattering by Obstacles*, D. Reidel, Dordrecht, the Netherlands, 1986.